Scientia Iranica (2024) 31(1), 26–42

Sharif University of Technology
Scientia Iranica
Transactions B: Mechanical Engineering
https://scientiairanica.sharif.edu

Improvement of the axial-jet-pump performance using modified mixing chamber configuration and inlet swirling flow

A.A.A. Sheha[a,b,*], K.A. Ibrahim[b], H.A. Abdalla[b], S.M. El-Behery[b], and I.M. Sakr[b]

a. *Mechanical Section Head PetroGulf Misr Petroleum Company, 10, St. 250 Sarayat El-Maadi, Cairo, Egypt.*
b. *Department of Mechanical Power Engineering, Faculty of Engineering, Menoufia University, Shebin El-Kom, Egypt.*

Received 1 December 2021; received in revised form 16 September 2022; accepted 21 February 2023

KEYWORDS
Computational fluid dynamics;
Flow-characteristics;
Mixing chamber configuration;
Swirl;
Axial-jet-pump performance.

Abstract. In the current research, numerical analysis was used to investigate the flow behavior through the axial-jet-pump with various mixing chamber configurations (straight pipe and straight pipe-diffuser-straight pipe) in the presence of inlet swirling flow and its influence on the pump performance. The effects of introducing inlet swirling flow in the suction chamber and the motive flow line are numerically investigated. The optimum swirl angle in the suction chamber is found to be 45°, which yields the maximum pump efficiency of 38.08% for the second configuration of the mixing chamber system. Consequently, the inlet swirl generally decreases the desired mixing chamber length. Additionally, the new mixing chamber configuration enhances the mixing process compared with the traditional mixing chamber. On the other hand, imparting a swirl in the motive line inversely affected the pump performance. Engendering a swirl in the suction chamber causes an improvement of 12.76% in pump efficiency compared to the same pump configuration without a swirl. The optimum tailpipe diffuser angle is found to be 3°.

1. Introduction

Axial-jet-pump has a vital role in the field of petroleum production. It is a static machine with no moving parts and uses liquids or gases as a working motive medium to transport fluids. The advantages of an axial-jet-pump are as follows: It has a simple structure, hasn't any moving parts, has reliable performance, is easy to fabricate and repair, doesn't need initial priming earlier to start up, and has good sealing. It has been widely applied under special working environments of high pressure, high temperature, underwater, and in a vacuum. Axial-jet-pump has a frequent use in lots of engineering fields. The efficiency of the axial-jet-pump is strongly influenced by both pump operating and geometric parameters.

Schulz [1,2], and Raabe [3] performed the first draft of the jet pump according to the construction guidelines. Hefny [4] conducted an experimental study to inquire about the swirl intensity effect on the jet pump performance. His study demonstrated that the weak swirl intensity has no effect on the pump

*. *Corresponding author. Tel.: +201020247010*
E-mail addresses: engineer_sheha@yahoo.com and asheha@petrogulfmisr.com (A.A.A. Sheha)

doi: 10.24200/sci.2023.59489.6271

performance, and the performance parameters such as head ratio, mass flow rate ratio, and efficiency can be predicted with a reasonable agreement.

Gelany [5] conducted an experimental study to exhibit the swirl intensity effect on the jet pump performance using multiple jets. He came to the conclusion that the best swirl intensity, which yields the best pump performance, is achieved at a high number of nozzles with long or medium mixing chambers.

Shimizu et al. [6] experimentally studied the swirl effect in the driving jet of an annular-jet pump. Their study involved a comparison of the annular-jet pump in case of not introducing an inlet swirl to that of introducing an inlet swirl with several swirl intensities. The results revealed that a little increase in the efficiency is observed with a moderate swirl, a weak swirl has no effect on the efficiency and a sturdy swirl decadent the pump efficiency.

Guillaume and Judge [7] established an experimental test rig to discuss the effect of swirl on an annular-jet pump performance. Their study showed that an intensive swirl is detrimental to the pump's efficiency, whereas a moderate swirl increases efficiency up to a certain value. They concluded that efficiency gains occur when the entrainment between the secondary and primary fluids increases. Also, the study showed that a weak swirl has no effect on efficiency.

Zhou et al. [8] carried out a numerical study to show the effect of swirl on the jet pump efficiency. They used fluent commercial CFD software to paradigm the effect of swirling the primary jet. They found that pump performance decreases as the swirl angle increases. Also, their study clarified that introducing a moderate swirl flow results in the entrained fluid increasing, and hence, the jet pump's efficiency can be increased using this method.

Yamamoto et al. [9] calculated the performance of an annular-jet pump with and without an inlet swirl and studied the impact of the inlet swirl and the driving jet's flow field on pump efficiency. They used the calculated flow fields to evaluate performance characteristics such as head ratio, mass flow rate ratio, and efficiency and compared the results to experimental data measured by Shimizu et al. [6].

Panevnyk [10] devised a basic function-approximated analytical method for the allocation of kinematic characteristics for the flow in the mixing chamber part of a down-hole jet pump. He came to the conclusion that the pattern of distribution for the velocity in the jet pump mixing chamber was influenced by the design and operating conditions of the down-hole ejection system.

De Jesús Portillo-Vélez et al. [11] offered a more simplified computational design approach for maximizing the efficiency of an axial-jet-pump utilized in the extraction of oil, taking its operation and geometric factors into consideration. They came to the conclusion that under some circumstances, the hydraulic jet pump might increase the tested wells' operational efficiency by up to 24%. Their study demonstrated that the best divergence angle of the pump diffuser is 5.5°. They found that at the relative position of the driving nozzle $Z = 0.5$, the highest efficiency of 25.6% occurs.

Aldas and Yapici [12] studied numerically the effect of four turbulence models on the performance of the axial-jet-pump. They made a comparison of the experimental results with all model results. They reached the conclusion that the transition (SST) turbulence model produced better realistic findings than other turbulence models, according to the study comparison.

Wang et al. [13] conducted a numerical study to enhance the performance of the early annular jet pump and streamlined annular jet pump. Their research demonstrated that when the flow rate ratio exceeds 0.3, the efficiency of the streamlined annular jet pump is better than that of the early annular jet pump, with a maximum increase of 1.2%.

Brijesh and Sagar [14] studied experimentally the influence of jet pump diffuser angle on the pump performance. The findings of the experiments revealed that adjusting the diffuser angle has an impact on the performance of the jet pump. They came to the conclusion that the highest jet pump efficiency is at a diffuser angle of 5°, as the pump enhanced the secondary fluid maximum value.

Xiaogang et al. [15] investigated numerically the flow characteristics for both traditional and ameliorated annular-water-air-jet-pump. Their study improved the annular-water-jet-pump performance by 10% compared with the traditional pump.

Zhu and Liu [16] utilized the hybrid grid technique in order to investigate the pressure drawdown mechanism of the jet pump bit and subsequently constructed a unique annular-jet-pump bit. In order to minimize the pressure in the bottom hole, their research showed that the combination of pressure drawdown theory and vortex-jet-flow is preferable.

Wang et al. [17] investigated the effect of suction chamber geometry on the flow field of the annular jet-pump. They compared the streamlined suction chamber and the conical suction chamber on the pump performance by using the turbulence numerical simulation method. They came to the conclusion that the streamlined suction chamber is seamlessly connected to the throat without any abrupt corner changes, eliminating low pressure at the throat's input wall, improving wall pressure distribution, and reducing the risk of cavitation.

Xu et al. [18] introduced an optimization method for the annular-jet pump design using the blending of computational fluid dynamics simulation, the approximate Kriging model, and experimental data. Their

study showed that the mixing effect at the suction chamber outlet can be improved by decreasing the area ratio, but the frictional resistance increases.

Helios and Asvapoositkul [19] designed a water jet pump apparatus for a total of nine experimental cases with three different area ratios and three mixing chambers in order to examine the effect of geometrical parameters on the performance and loss coefficient of the mixing chamber and diffuser of the water jet pump. Their results announced the best efficiency was 23.37%, and the low area ratio and the small mixing chamber resulted in the best loss coefficient.

Murillo et al. [20] used genetic algorithm methods for the optimizations of jet pump geometrical parameters used in ethanol vacuum distillation. They concluded that the performance parameters of jet pumps are importantly affected by the inlet pressure for all jet pump optimizations.

Wang et al. [21] conducted a numerical analysis to determine how an annular jet pump's cavitation performance is affected by the suction chamber and the mixing chamber intake characteristics. The findings demonstrated that employing the streamlined annular jet pump can boost jet pump efficiency. The biggest improvement was 1.4%.

Gao et al. [22] simulated the impact of the suction chamber half-angle on jet pump performance. Their findings demonstrated that the jet pump performance was significantly impacted by the suction chamber half-angle.

Xu et al. [23] optimized the annular jet pump performance. They investigated the effect of design parameters such as suction chamber angle, diffuser angle, area ratio, and flow rate ratio on the pump performance. Their optimization study increased the pump head ratio by 30.46%. Their suggested technique of pump performance optimization serves as a model for enhancing the efficiency of other pumps.

Toteff et al. [24] conducted a numerical study to optimize a booster multiphase jet pump system placed in a conventional heavy oil system. Their study revealed that the optimized pump provides a significant 17% increase in total flow capacity over the original. Their optimization study showed that fluid production goes up by 30% with the best geometrical parameters.

It appeared from the literature survey that most numerical and experimental studies were conducted in this field to get the maximum efficiency. It seems that research studies on the influence of the mixing chamber configuration as a mixing duct system (straight pipe-diffuser-straight pipe) and the effect of inlet swirl strength at the entrained fluid on the performance of axial-water-jet-pumps are very few investigated. As a result, the major goal of the current numerical study is to determine the impact of modified mixing chamber configuration (straight pipe-diffuser-straight pipe) and inlet swirl intensities in the suction chamber and the motive line on the performance of axial-water-jet-pump.

2. Jet pump flow modelling

2.1. The physical model

The used axial-jet-pump configuration is displayed in Figure 1, with an illustration of all pump parts. The schematic of the pump is shown in Figure 2. The cross-section of the pump is circular at all points. The inner surfaces of all sections of the pump are assumed to be smooth in the current study ($K_s = 0.00015$ mm). The Design Modeler software adopted in ANSYS® Fluent, Release 17.0 [25] is used to design the various case dimensions of the axial-jet-pump 3D solid modeling with a two-stage diffuser.

2.2. The numerical model and methodology

The present numerical study is adopted as a CFD commercial code (ANSYS® Fluent, Release 17.0), which employs a finite volume discretization and stratifies 3D-RANS (Reynolds-Averaged-Navier-Stokes equations) technique. The numerical simulations of water flow through the axial-jet-pump are carried out using 3D steady flow. The procedure of solution is an implicit iterative method based on finite volume discretization and employs a solution algorithm created specifically for single-phase flow and loosely based on the SIMPLE algorithm. To solve the nonlinear system of discretized equations, a finite volume discretization technique is utilized, and an iterative method is applied. SIMPLE technique algorithm is used for the coupling of pressure-velocity. All grids are structured and have been generated using the ANSYS Meshing program. The axial water-jet-pump numerical simulation is being held to simulate the flow behavior through the pump and anticipate the performance of the axial-water-jet-pump using the mixing duct system as (straight pipe and straight pipe-diffuser-straight pipe), inlet swirl with various degrees of swirl in the suction chamber and in the motive line. The transition SST model is utilized, as recommended by prior studies of [12,26,27]. This turbulence model reasonably showed agreement between numerical and experimental results. As a result of the very complex flow through the axial-water-jet-pump, the next assumptions are established to assess the flow of the water through the pump: (i) The flow is incompressible; (ii) The flow within the axial-jet-pump is steady; (iii) Between the surroundings and the water, no heat transfer occurs; and (iv) The surface roughness effect is negligible ($K_s = 0.00015$ mm). The operating equations are foreordained as follows:

In the case of incompressible flow, the Reynolds-averaged continuity equation and momentum equation are:

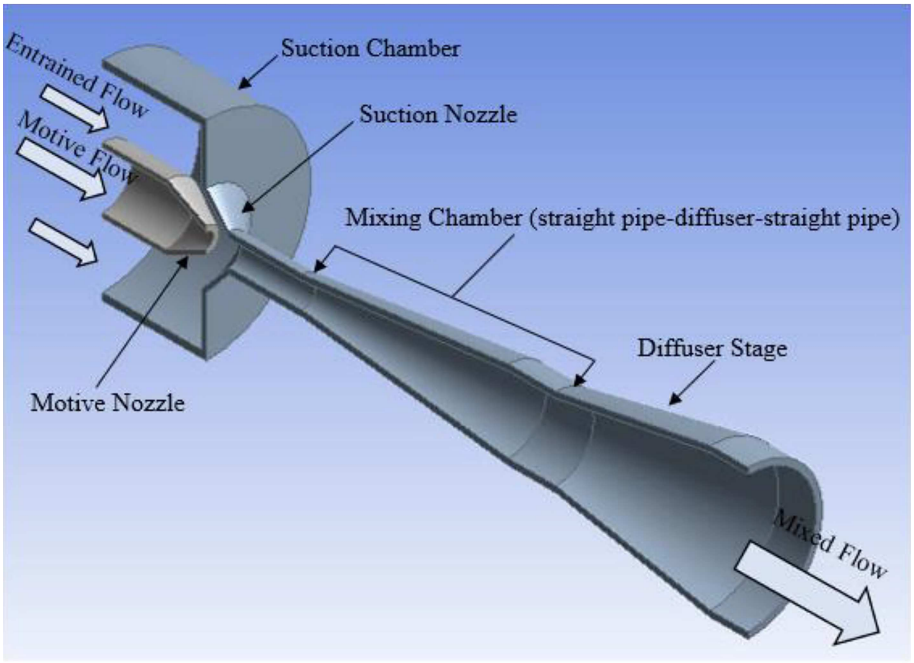

Figure 1. Geometric parameters of tested axial-jet-pump with modified mixing chamber system.

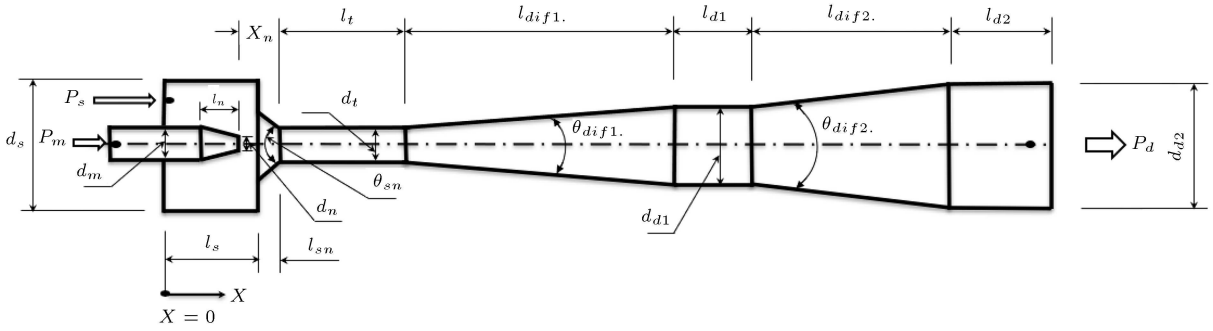

Figure 2. Characteristic dimensions of the axial-jet-pump geometry using a modified mixing chamber system.

$$\frac{\partial \rho}{\partial t} + \frac{\partial (u_i)}{\partial x_j} = 0, \tag{1}$$

$$\frac{\partial (\rho u_i)}{\partial t} + \rho \frac{\partial (u_i u_j)}{\partial x_j} = \frac{\partial}{\partial x_j}\left[\mu \frac{\partial u_i}{\partial x_j}\right] + \frac{\partial \tau_{ij}}{\partial x_j} - \frac{\partial p}{\partial x_i}, \tag{2}$$

where the Reynolds stress is:

$$\tau_{ij} = -\rho \overline{u_i` u_j} = \mu_\tau \left[\frac{\partial u_i}{\partial x_j} + \frac{\partial u_j}{\partial x_i}\right] - \frac{2}{3} k \rho \delta_{ij}, \tag{3}$$

where (ρ) is the fluid density, and (μ) is the dynamic viscosity. The turbulent Prandtl number Pr_t is computed based on the turbulent viscosity μ_t. The term $-\rho \overline{u_i` u_j}$ in Eq. (2) is defined as Reynolds-stress-tensor. The term ($`u_i$) is the fluctuating velocity, and the term (u_i) is the mean velocity, where both terms are in the direction (i).

Four equations represent the turbulence model (transition-SST). A detailed description of (transition-SST) turbulence models can be found in the ANSYS theory guide [25]. The equations of turbulence models are clarified as follows:

The equation of intermittency-transport (γ) is:

$$\frac{\partial (\rho \gamma)}{\partial t} + \rho \frac{\partial (\rho u_i \gamma)}{\partial x_j} = -E_{\gamma 1} + P_{\gamma 1} - E_{\gamma 2} + P_{\gamma 2} + \frac{\partial}{\partial x_j}\left[\left(\mu + \frac{\mu_\tau}{\delta_Y}\right)\frac{\partial \gamma}{\partial x_j}\right], \tag{4}$$

where ($E_{\gamma 1}$ and $P_{\gamma 1}$) are transition sources, and ($E_{\gamma 2}$ and $P_{\gamma 2}$) are destruction source and relaminarization source.

The transport equation for transition momentum thickness Reynolds number $\tilde{Re}_{\theta t}$, that clarify criteria

for transition onset is:

$$\frac{\partial\left(\rho\,\tilde{R}e_{\theta t}\right)}{\partial t}+\frac{\partial\left(\rho u_j\,\tilde{R}e_{\theta t}\right)}{\partial\,x_j}=P_{\theta t}+\frac{\partial}{\partial\,x_j}\left[\sigma_{\theta t}\left(\mu+\mu_\tau\right)\frac{\partial\left(\tilde{R}e_{\theta t}\right)}{\partial\,x_j}\right], \tag{5}$$

where $(P_{\theta t})$ is the source term and is defined as follows:

$$P_{\theta t}=c_{\theta t}\,\frac{\rho}{t}\left(\mathrm{Re}_{\theta t}-\tilde{R}e_{\theta t}\right).\left(1.0-F_{\theta t}\right), \tag{6}$$

$$t=\frac{500\mu}{\rho\,U^2}, \tag{7}$$

$$F_{\theta t}=\min\left(\max\left(F_{wake}\,e^{\left(-\frac{y}{\delta}\right)^4},1.0-\left(\frac{y-1/50}{1.0-1/50}\right)^2\right),1.0\right), \tag{8}$$

$$F_{wake}=e^{-\left(\frac{\mathrm{Re}_\omega}{1E+5}\right)^2}, \tag{9}$$

$$\mathrm{Re}_\omega=\frac{\rho\omega\,y^2}{\mu}. \tag{10}$$

The model constants for the $\tilde{R}e_{\theta t}$ equation are $c_{\theta t}$ and $\sigma_{\theta t}$ that have the following values [25]:

$$c_{\theta t}=0.03,\qquad \sigma_{\theta t}=2.0.$$

The turbulence kinetic energy transport equation for (k) is:

$$\frac{\partial}{\partial\,x_j}\left(\rho\,u_j\,k\right)=-\tilde{D}_k+\gamma_{eff}\,\tilde{P}_k+\frac{\partial}{\partial\,x_j}\left[\left(\mu+\sigma_k\,\mu_t\right)\frac{\partial k}{\partial\,x_j}\right], \tag{11}$$

where $\tilde{D}_k$ (the destruction term) and $\tilde{P}_k$ (the production term) for the turbulence model are defined by the terms as follows:

$$\tilde{P}_k=\min\left(P_k,10\rho\beta*k\omega\right), \tag{12}$$

$$\tilde{D}_k=\min\left(\max\left(\gamma_{eff},1.0\right),1.0\right)D_k, \tag{13}$$

$$D_k=\rho\beta*k\omega. \tag{14}$$

The specific dissipation rate transport equation for (ω) is:

$$\frac{\partial}{\partial t}\left(\rho\omega\right)+\frac{\partial}{\partial\,x_j}\left(\rho u_j\,\omega\right)=\alpha\frac{\tilde{P}_k}{\upsilon_t}+Cd_w-D_w+\frac{\partial}{\partial\,x_j}\left[\left(\mu+\sigma_w\,\mu_t\right)\frac{\partial\omega}{\partial\,x_j}\right], \tag{15}$$

where D_w is the dissipation term and Cd_w is the cross-diffusion term for ω, respectively. More specifics are found in [28–30].

The workflow process of the current research and the procedures for improving the axial-jet-pump performance are shown in Figure 3.

3. Mesh quality test

In the present numerical study, special quality measures and considerations are applied to the generated mesh in order to obtain stable and reliable CFD results with acceptable accuracy measures before moving to the step of solver order. Three indicators are used in the present study in order to report the mesh quality, as shown in Table 1.

4. Near wall treatment

The maximum y^+ value is less than 5, and its value beside the pump's outer wall ranges from 0.08 to 0.94 along the pump, as shown in Figure 4. Hence, the near wall region is treated as a viscous sub-layer region. In the present numerical study, a first layer thickness of $(0.2\times10^{-3}$ m) is used near the pump outer wall. In order to improve the boundary layer simulation accuracy, an inflated mesh is used near the wall frontiers. An inflated meshing procedure with eight layers of prismatic inflation with a growth rate of 1.2 was used in the near-wall region.

The following parameters are used to describe the performance of jet pumps:

(i) The mass flow rate ratio (M_r):

$$M_r=\frac{\dot{m}_s}{\dot{m}_m}. \tag{16}$$

(ii) The pressure ratio (P_r):

$$P_r=\frac{(P_d-P_s)}{(P_m-P_d)}. \tag{17}$$

Table 1. The mesh quality measures used in the study.

Parameter of quality	Value of mesh	Limitation values
Aspect ratio	2.4846	(0–100)
Orthogonal quality	0.9167	(0–1)
Skewness	0.2318	(0–1)

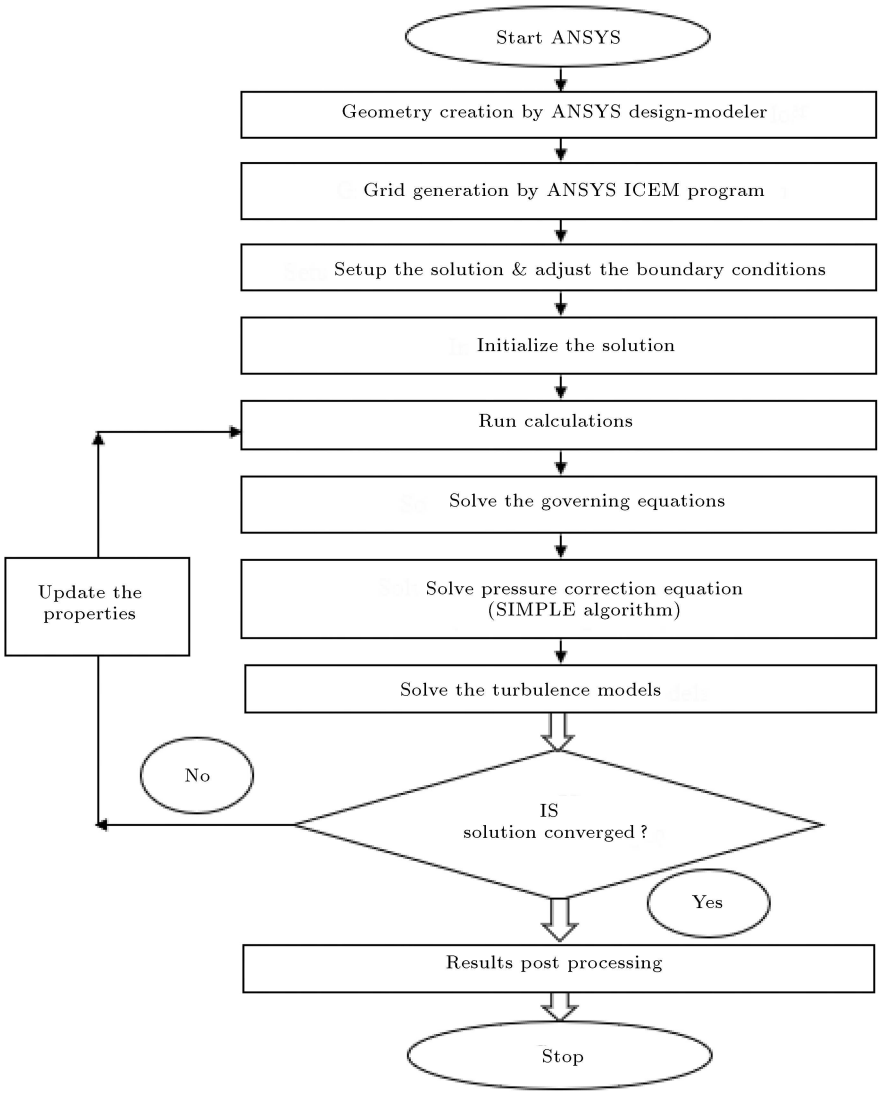

Figure 3. The flow chart indicates the computational procedures of the current study.

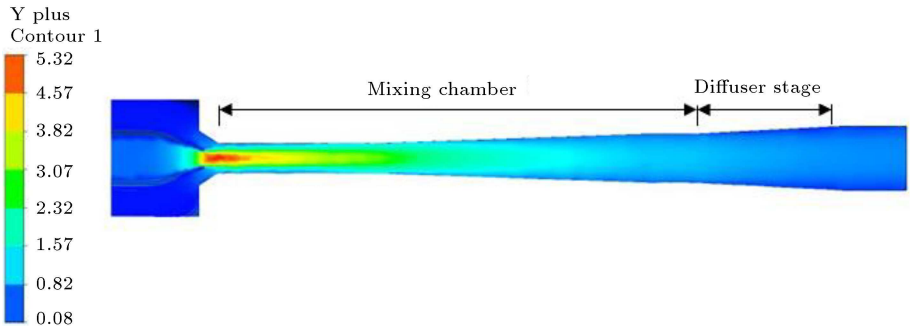

Figure 4. y^+ contour for the computational domain.

(iii) The jet pump efficiency (η):

$$\eta = M_r \cdot P_r \cdot \tag{18}$$

5. Grid independent study

Because of the symmetry of axial-jet-pumps, instead of using the complete pump, half of it is used as the computational zone in the simulation. Three different meshes are tested to ensure grid-independent results. A fine grid is performed near the inner and outer walls due to steep variations in the variables (u, t, etc.), as illustrated in Figure 5. Aside from non-straight walls, mesh inflation is used. The computations are

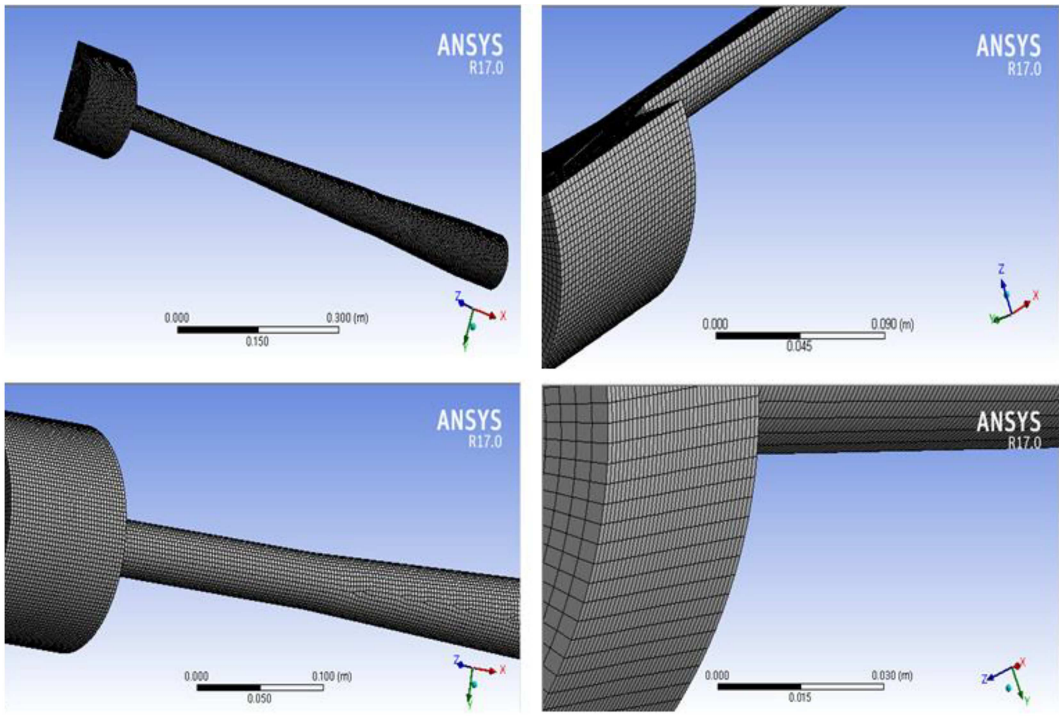

Figure 5. Generated structured mesh.

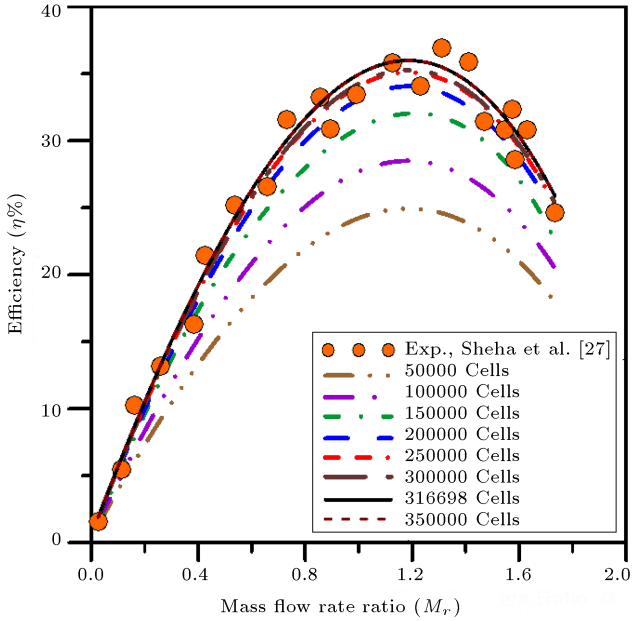

Figure 6. Grid independent study for the present numerical study.

performed for 316698 cells in the current investigation to ensure grid-independent results.

Figure 6 shows the grid-independent study, which illustrates the number of cells after which the solution remains constant, but the computational time increases. Also, the figure shows the agreement between the CFD, 3D technique, and experimental data for a pump with the same dimensions and operating conditions.

The CFD, 3D technique, and turbulence model (Transition SST) are used in the present numerical investigation despite the long computational time in order to help save efforts exerted in laboratories for predicting one or more operational and geometrical parameters.

6. Results and discussion

The numerical outcomes of several modifications are analyzed in this section. The comparisons are carried out under identical operating conditions, while the pump geometries are mentioned in each section. In the present study, the motive mass flow rates are assorted from (1.863 kg/s) to (8.859 kg/s), the suction mass flow rates are assorted from (0.207 kg/s) to (14.553 kg/s), the suction pressure values were assorted from (−36000 Pa) to (25000 Pa), and the motive pressure values are assorted from (101325 Pa) to (486847 Pa).

6.1. The validation of the present numerical code

In the current study, comparisons were carried out between the present computational outcomes and experimental and numerical data of Aldas and Yapici [12] at the identical dimensions of the jet pump and the identical boundary conditions. The boundary conditions

Table 2. Boundary conditions were used in the comparison with Aldas and Yapici [12].

P_m (Pa)	P_s (Pa)	P_d (Pa)
486829	−11000	123913
486829	−11000	122946
486847	−18000	103563
481851	−27000	84139
481887	−30500	76424
482896	−36000	69618
231793	−18000	29354
220749	−12500	30403
202636	−4000	31433
195614	1500	32489
187547	7000	33489
132542	18500	34534
162426	25000	35601
162412	24000	33590

used in the validation are listed in Table 2. Figure 7 displays the pump efficiency and pressure ratio with the mass flow rate ratio using experimental and numerical results. As shown in Figure 7(a), the efficiency of the pump increases, demonstrating a summit at about $M_r = 1.72$, and then decreases with the mass flow rate ratio increasing. Figure 7(b) indicates that when the mass flow rate ratio increases, the pressure ratio in jet pumps drops almost linearly. Because the low-energy entrained fluid and the motive fluid mix, this is a predicted behavior. In the range of mass flow rate ratios from 1.2 to 2.75, the current numerical results are quite similar to the experimental and numerical results obtained by Aldas and Yapici [12]. Furthermore, in the regions of summit efficiency and high mass flow rate ratios, the current 3D numerical results match the experimental data better than the 3D results of Aldas and Yapici [12].

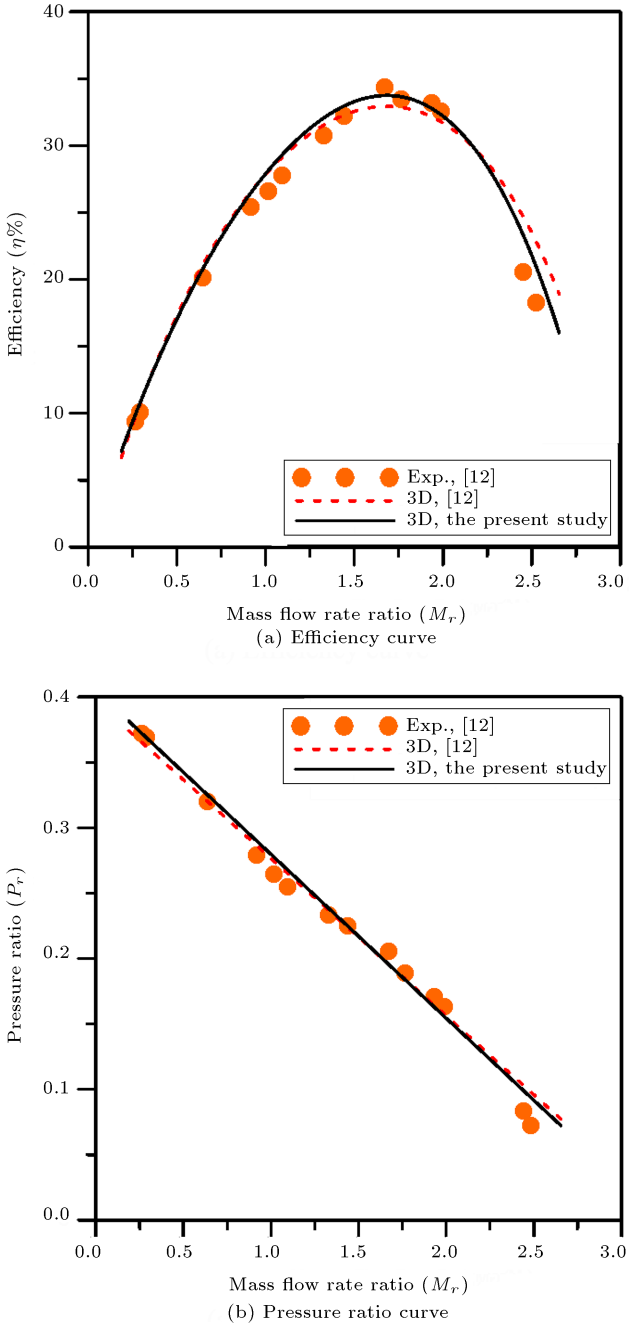

Figure 7. Comparison of the current CFD results with Aldas and Yapici's experimental and CFD results [12].

6.2. Swirl effect on the jet pump performance

Several degrees of swirl were applied in the motive line and the suction chamber for the same model dimensions and the same boundary conditions of Sheha et al. [27] and Sheha [26] to research the swirl effect on jet pump performance. The boundary conditions that used in the present numerical study are listed in Table 3. In the present study, the swirl generation is adopted in the CFD code by the direction specification method. In this method, the mean flow direction with respect to the coordinate system is specified after analyzing the suction flow at the inlet of the suction chamber via Tangential-Flow-Direction-Component and Axial-Flow-Direction-Component. The Direction-Vector is selected as Direction-Specification-Method. The Local-Cylindrical (Radial, Tangential, and Axial) is selected as Coordinate-System. Finally, the flow is analyzed as sin (swirl angle) and cos (swirl angle). The swirl velocity is calculated via numerical results after the solution is completed and converged.

6.2.1. Effect of adding swirl in suction chamber on axial-jet-pump performance with straight mixing chamber configuration

The effect of the inlet swirl in the suction chamber

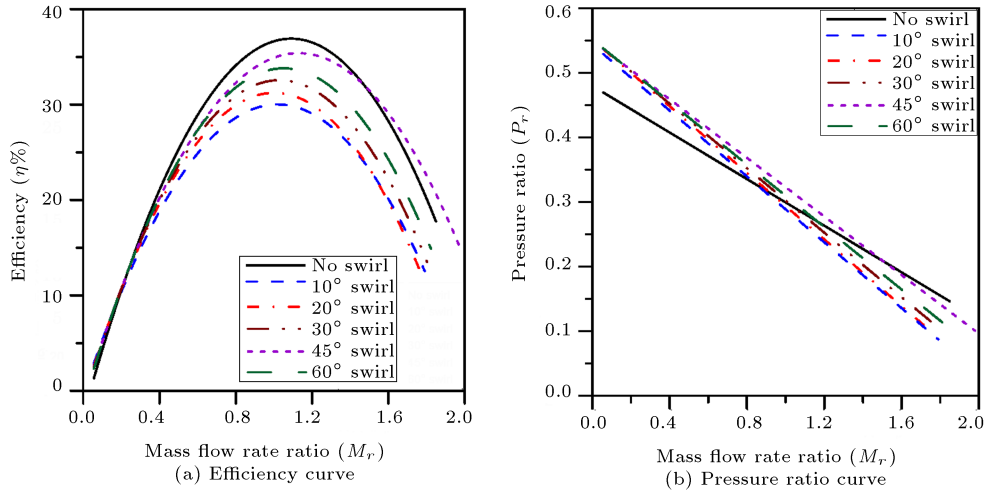

Figure 8. The effect of the degree of swirl in the suction chamber on the pump efficiency and pressure ratio.

Table 3. Values of boundary conditions used in the present numerical study [26].

P_m (Pa)	P_s (Pa)	P_d (Pa)
101325	1500	14185.5
121590	1500	20265
141855	1500	25331.3
162120	1500	30397.5
182385	1500	42556.5
202650	1500	43063.2
243180	1500	43569.8
263445	1500	44076.4
374902.5	1500	49649.3
506625	1500	55728.8
182385	981	45596.3
182385	981	50662.5
182385	981	55728.8
182385	981	60795
182385	981	65861.3
182385	981	68901
182385	981	70927.5
182385	981	71940.8
182385	981	74980.5

on the axial-jet-pump performance is numerically investigated. When a swirling flow is introduced to the suction chamber of the axial-jet-pump with a straight mixing chamber configuration, the pump efficiency increases up to a certain value depending on the degree of the inlet swirl. After that, the pump efficiency decreases with increasing the degree of swirl.

As shown in Figure 8(a), degrees of swirl ranging from 10° to 60° are engendered in the suction chamber. The 45-degree swirl increases the pump operating range and shows the highest efficiency compared with other degrees of swirl, but the peak efficiency value is still lower than the value in case of no swirl. The pressure ratio curve for several degrees of swirl in the suction chamber can be shown in Figure 8(b). As the mass flow rate ratio increases, the pressure ratio drops linearly for a constant swirl angle. It is observed for mass flow rate ratio below 1.0 that the pressure ratio increases with increasing the swirl strength. The results indicate that, for swirl angle equals 45°, the pressure ratio has higher values compared with the case of no swirl up to $M_r = 1.4$ as the 45° swirl results in the suction pressure decreasing.

6.2.2. Effects of adding swirl in motive line on axial-jet-pump performance with straight mixing chamber configuration

The effect of imparting swirl in the motive line on the axial-jet-pump performance is numerically investigated. When swirling flows are introduced to the motive line of the jet pump with a straight mixing chamber configuration, the pump efficiency decreases by increasing the degree of the inlet swirl.

As shown in Figure 9(a), degrees of swirl ranging from 10° to 50° are engendered in the motive line. The engendered swirl flows badly affected the pump efficiency, as the swirl flow resulted in pressure losses in the motive jet. The presence of swirl flow in the jet pump shifts the peak of efficiency to a higher mass flow ratio as the swirl strength is increased. The pressure ratio curve for the several degrees of swirl engendered in the motive line can be shown in Figure 9(b). The results show a monotonic decrease for both swirling and non-swirling flow cases. It is observed for mass flow rate ratio below 0.5 that the pressure ratio increases with increasing the swirl strength. Afterwards, the pressure ratio decreases linearly with increasing the swirl intensity.

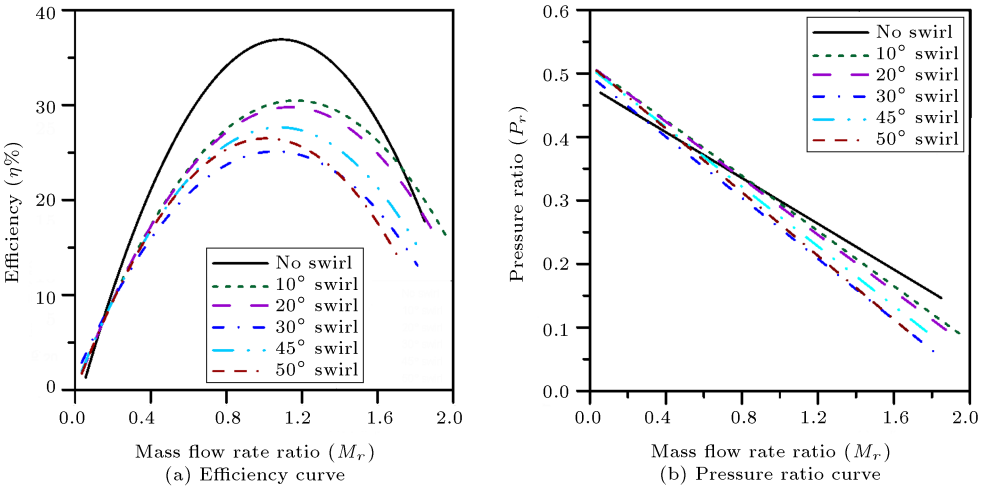

Figure 9. The effect of the degree of swirl in the motive line on the pump efficiency and pressure ratio.

Table 4. Dimensions for the several configurations of the modified mixing chamber system, including the optimum configuration.

Geometry	l_s	d_s	l_{sn}	θ_{sn}	l_n	d_m	d_n	l_t	d_t	$l_{dif1.}$	$\theta_{dif1.}$	l_{d1}	d_{d1}	$l_{dif2.}$	$\theta_{dif2.}$	l_{d2}	d_{d2}
G1	110	152.4	25	86°	60	60	19	200	36.5	83.61	8°	6 0	60	56.71	10°	80	80
G2	110	152.4	25	86°	60	60	19	200	36.5	111.79	6°	72	60	71.15	8°	80	80
G3	110	152.4	25	86°	60	60	19	200	36.5	168.03	4°	20	60	95.14	6°	80	80
G4	110	152.4	25	86°	60	60	19	200	36.5	336.48	2°	60	60	143	4°	80	80
G5	110	152.4	25	86°	60	60	19	200	36.5	336.48	2°	60	60	190.8	3°	80	80
G6	110	152.4	25	86°	60	60	19	200	36.5	673.16	1°	60	60	286.4	2°	80	80
G7	110	152.4	25	86°	60	60	19	200	36.5	–	–	–	36.5	485	5°	90	80

All dimensions are in (mm).

6.3. Effect of mixing chamber configuration (straight pipe-diffuser-straight pipe) on axial-jet-pump performance

In jet pumps, the motive and entrained flows are mixed in a flow path called the mixing chamber. Numerous factors, such as the geometry and shape of the chamber entry and the mixing chamber, affect the momentum exchange between the two flows and, as a result, the degradation of core flow velocity. The mixing chamber's goal is to achieve a higher mixing rate with minimal primary flow losses across a limited total length. In the present study, a modified mixing chamber configuration (straight pipe-diffuser-straight pipe) is utilized to ameliorate the axial-jet-pump performance. Several configurations of the new modified mixing chamber configuration comprised several angles for mixing diffuser elements ranging from 1° to 8° and comprised several angles for tailpipe diffuser elements ranging from 2° to 10° respectively, as mentioned in Table 4. It can be noticed in Figure 10(a) that the modified mixing chamber configuration (Straight pipe-diffuser-straight pipe) with small tailpipe diffuser angles and some extent of long pressure recovery length result in a significant improvement in pump efficiency and pressure ratio and increase the pump operating range. The reason for the pump performance improvement dates back to the better mixing process and lower mixing losses through the modified mixing chamber system compared with the straight pipe mixing chamber. In addition, the swirl generation at the inlet of the suction chamber improves the mixing process through mixing chamber configuration and results in separation devastation in the diffuser stage. The fluid behavior and the flow regimes through the axial grooves can be obtained in detail from Refs. [31,32]. The analysis of the fluid-structure interaction can be found in [33].

The configuration (G5) with a 3° tailpipe diffuser angle shows better pump performance compared with other configurations. Engendering a swirl in the suction chamber with 45° of swirl at the configuration (G5) increases the pump performance, and pump efficiency reaches 38.08%, in addition to the increase of pump operating range. The pressure ratio curve for the several configurations of the modified mixing chamber system can be shown in Figure 10(b).

It can be noticed from Figure 10 that the effi-

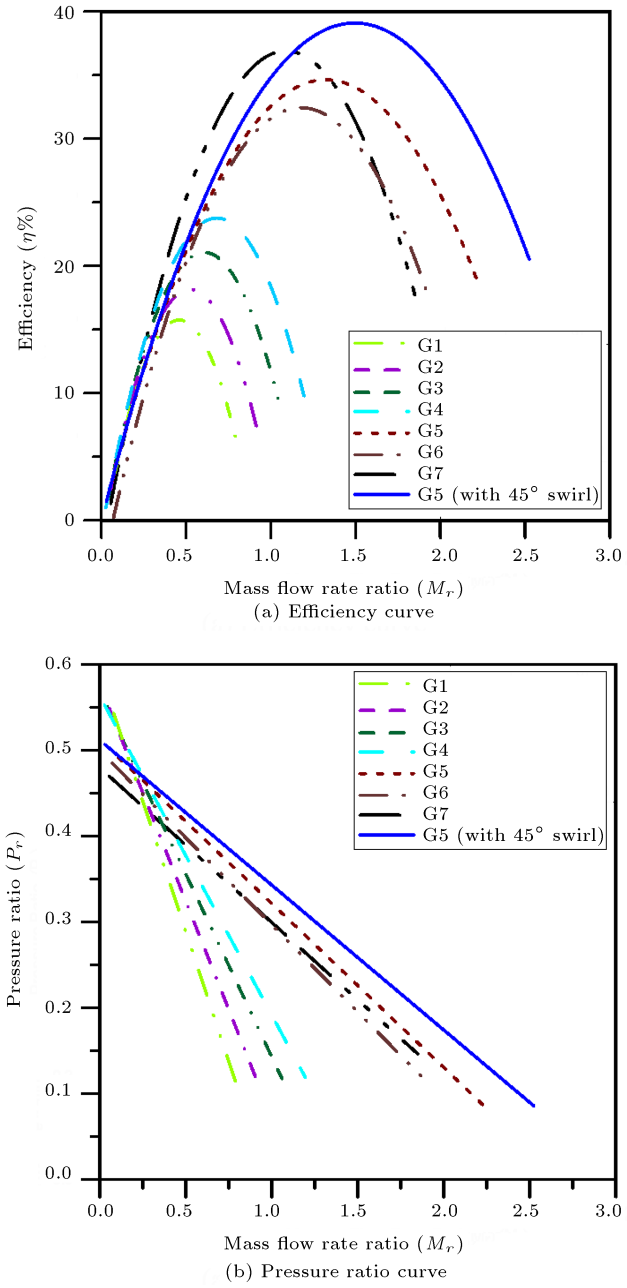

Figure 10. The effect of a modified mixing chamber system on the pump efficiency and pressure ratio.

ciency and pressure ratio characteristics of G1, G2, G3, and G4 are significantly different from those of G5, G6, and G7. The reason for this difference is that the configurations G1, G2, G3, and G4 have a higher value for diffuser angle that results in a separation through diffuser stages, which decreases the axial-jet-pump efficiency and pressure ratio. The configurations G5 and G6 have a lower value for diffuser angle that devastated the separation in the diffuser stages, which increases the axial-jet-pump efficiency and pressure ratio. The configuration G7 has a straight pipe mixing chamber and one diffuser stage with an angle (5°) that is recommended by a previous study, which devastates the separation in the diffuser stage and increasingly affects the axial-jet-pump efficiency and pressure ratio. Finally, the configuration (G5) with a 3° tailpipe diffuser angle shows better pump performance compared with other configurations.

Figure 11 illustrates the velocity distribution and streamlines while generating a swirl in the motive line and the suction chamber of the configuration system (G7) with a mixing chamber (straight pipe) for the same 1:1-scale of [27]. As shown in Figure 11(a), it is observable that the inlet swirl in the motive line badly affects the pump performance and results in losses in the motive jet velocity. The losses in the motive jet velocity result in a decrease in the vacuum created in the suction chamber that decreases the rate of the entrained fluid. Also, the inlet swirl in the motive line results in separation in the whole length of the diffuser stage that extends to the diffuser exit. So, the pump performance is decreased. As shown in Figure 11(b), the inlet swirl in the suction chamber improves the pump performance. The swirl results in the entrained fluid increasing for a certain motive flow rate. Furthermore, the input swirl in the suction chamber wreaks havoc on the separation formation in the two diffuser stages. Additionally, the mixing of the motive and entrained fluids in the mixing chamber and diffuser is greatly aided by the shear layers produced by the swirl flow. Consequently, the inlet swirl is recommended in the pump suction chamber.

Figure 12 illustrates the velocity distribution and streamlines for the modified mixing chamber configuration system (straight pipe-diffuser-straight pipe) with a 3° tailpipe diffuser angle in case of generating a swirl in the suction chamber and without generating a swirl in the suction chamber. It can be noticed from Figure 12(a) and (b) that the velocity range, velocity distribution, velocity streamlines, and velocity contours are almost the same. The reason for this similarity is that the two cases are at the same boundary conditions and the same geometry. As shown in Figure 12(a), it can be noticed that creating a swirl with the degree of swirl (45°) increased the rate of entrained fluid for the same value of motive flow rate. Further, the 45° inlet swirl in the suction chamber devastated the formation of separation in the diffuser stage. As shown in Figure 12(b), the absence of an inlet swirl in the suction chamber decreased the rate of the entrained fluid. Therefore, the 45° inlet swirl is recommended in the suction chamber.

6.4. Swirl intensity

The intensity of the swirl is measured by the swirl number, which is a non-dimensional parameter. The ratio of the angular momentum's axial flux to the axial momentum's axial flux is known as the swirl

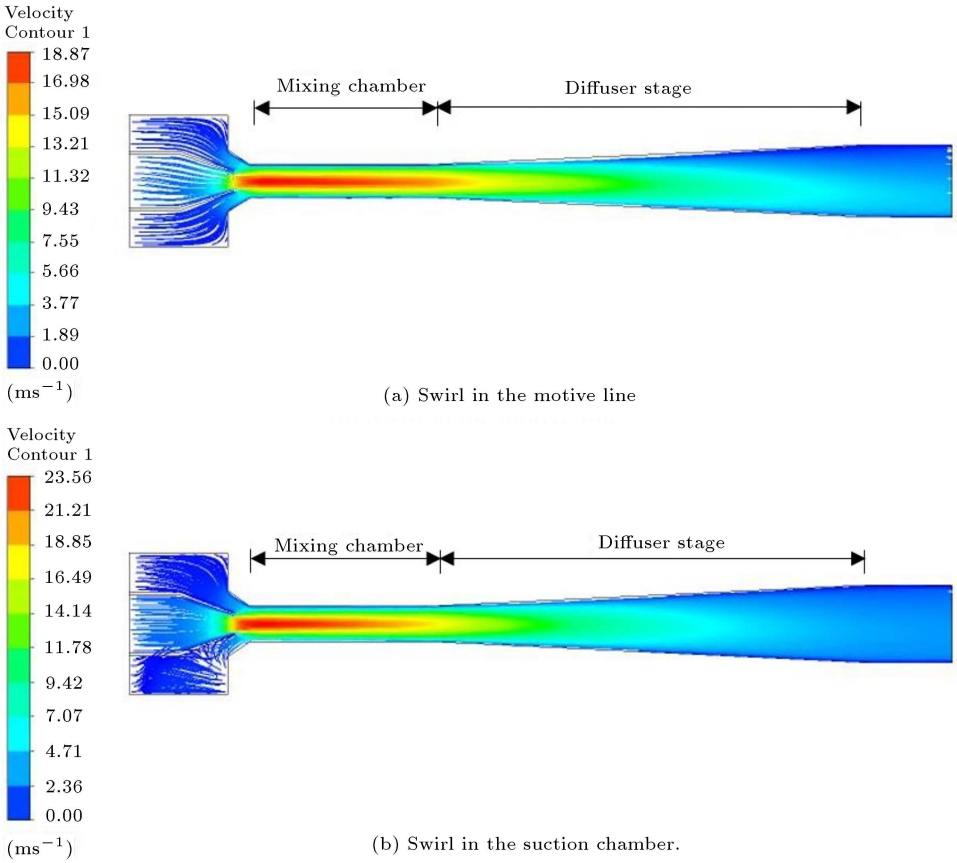

Figure 11. Velocity distribution and streamlines for configuration system (G7) with the same degree of swirl (45°) and the same boundary conditions.

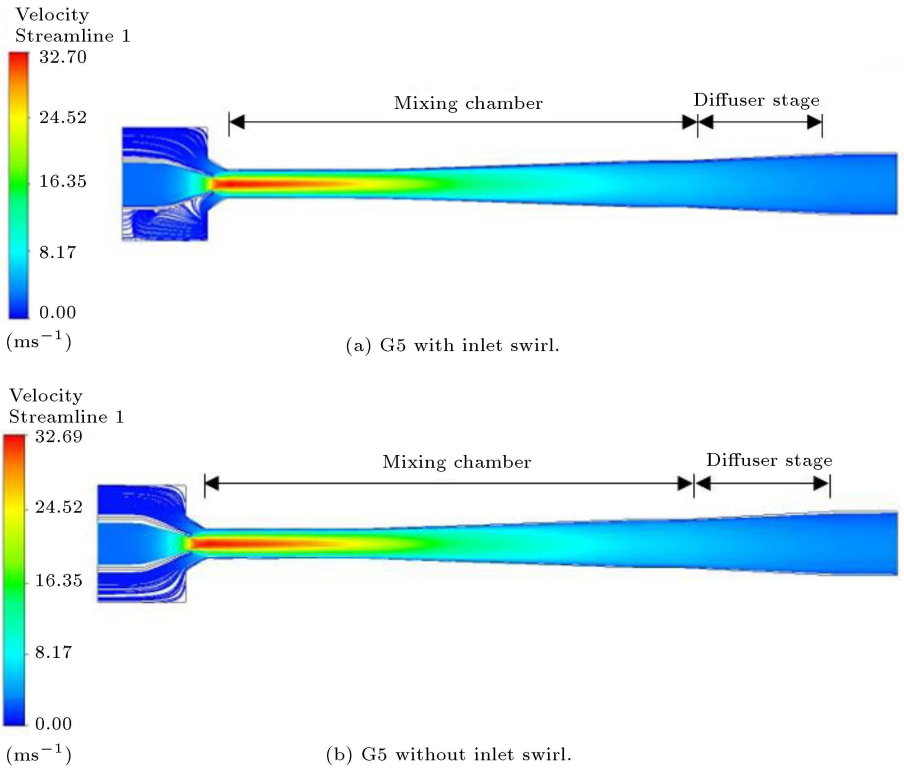

Figure 12. Velocity distribution and streamlines for the optimum modified mixing chamber configuration system (G5: with and without inlet swirl).

number [34]. It can be represented as follows:

$$S = \frac{2\pi\rho \int_0^{R_0} r^2 v_z v_\theta dr}{2\pi\rho R_0 \int_0^{R_0} r v_z^2 dr}, \quad (19)$$

where r is the radial coordinate, R_0 is the radius at the pump cross-sectional surface, v_z is the axial velocity, v_θ is the tangential velocity, and θ is the azimuthal angle on the cross-sectional surface.

Figure 13 illustrates the swirl number along the axial-jet-pump in case of creating an inlet swirl in the suction chamber with a 45° inlet swirl and without creating a swirl in the suction chamber. The pump dimensions are for configuration G5, and the detailed dimensions are mentioned in Table 4. It can be seen that the swirl number in the case of generating an inlet swirl in the suction chamber is higher than the swirl number in case of the absence of an inlet swirl along the suction chamber, the suction nozzle and the first quarter of the mixing chamber. The swirl number value at the inlet of the suction chamber reached up to 0.675 in the case of generating an inlet swirl. Therefore, the 45° inlet swirl results in the entrained fluid increasing for the same motive flow rate.

Figure 14 illustrates the velocity distribution contours and streamlines along the axial-jet-pump with several configurations of a modified mixing chamber system. These configurations are studied at the same throat inlet diameter and the same values of inlet and outlet diameters for the tailpipe diffuser (d_t = 36.5 mm, d_{d1} = 60 mm, and d_{d2} = 80 mm).

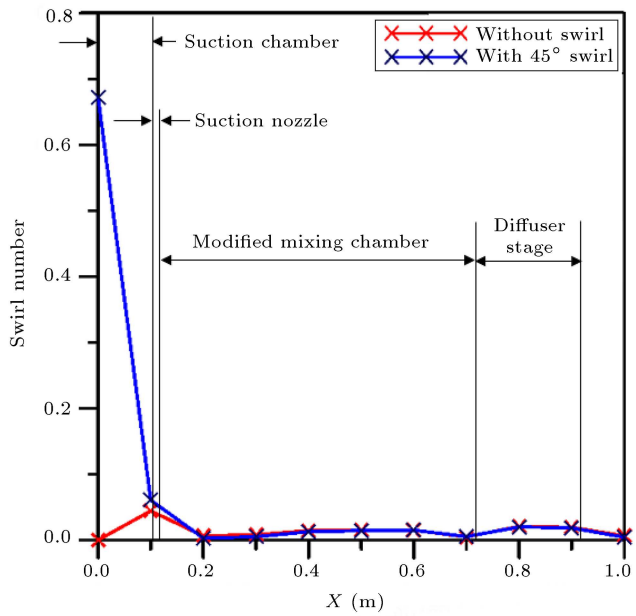

Figure 13. Swirl number along the axial-jet-pump for the optimum modified mixing chamber configuration system (G5: with 45° inlet swirl and without inlet swirl).

It can be seen that increasing the angle of the diffuser stage and decreasing pressure recovery length results in a separation in the diffuser stage, which extends to the diffuser exit, as shown in Figure 14(a). Also, it can be noticed that decreasing the angle of the diffuser stage and increasing pressure recovery length cause a reduction of the separation size in the diffuser stage, as displayed in Figure 14(b)–(d). The modified mixing chamber configuration (G5) with a tailpipe diffuser angle (3°) showed better pressure recovery and the best pump performance in addition to the process through the whole pump is without any separation in the modified mixing chamber system and the tailpipe diffuser as shown in Figure 14(e). On the other hand, decreasing the angle of the diffuser stage and increasing the pressure recovery length with values greater than the optimum value (3°) results in high friction losses and decreases the pressure recovery, causing a decrease in the pump performance, as shown in Figure 14(f). It's observable in Table 4 that the suction chamber sizes of G1 ∼ G6 are the same. However, in Figure 14, there are significant differences in the structural dimensions of each model. The reason for these significant differences in the structural dimensions of each model dates back to the different configurations of the tailpipe diffuser, as all diffusers do not have the same recovery length. In order to keep the same diffuser inlet and outlet diameter, the diffuser length increases by decreasing its angle, and this affects all parts in the cloud image decreasingly.

The pressure distribution along the axial-jet-pump outer surface is shown in Figure 15, with various modified configurations of the mixing chamber system.

In comparison to other designs, the configurations (G5 and G6) introduce the best vacuum pressure in the suction nozzle, resulting in higher entrained fluid. Furthermore, (G5) exhibits greater pressure recovery than (G6). Consequently, the highest efficiency and optimum performance are attained at the design (G5). It should be observed that the pressure at the suction nozzle for the configurations (G4, G5, and G6) is even lower than (−20,000 Pa), but cavitation doesn't happen because the negative pressure value along the suction nozzle doesn't approach the vapor pressure of water at the operating temperature. Additionally, the axial-jet-pump is submersed in water since the boundary conditions utilized are the same as those of Refs. [26,27].

Figure 16 illustrates the pressure distribution along the center line of the axial-jet-pump with several configurations of a modified mixing chamber system. Along the suction nozzle and the majority of the mixing chamber, the pressure for the configurations (G5 and G6) declines to a lower value than for the other configurations, then abruptly rises along the mixing chamber exit and tailpipe diffuser. The configurations

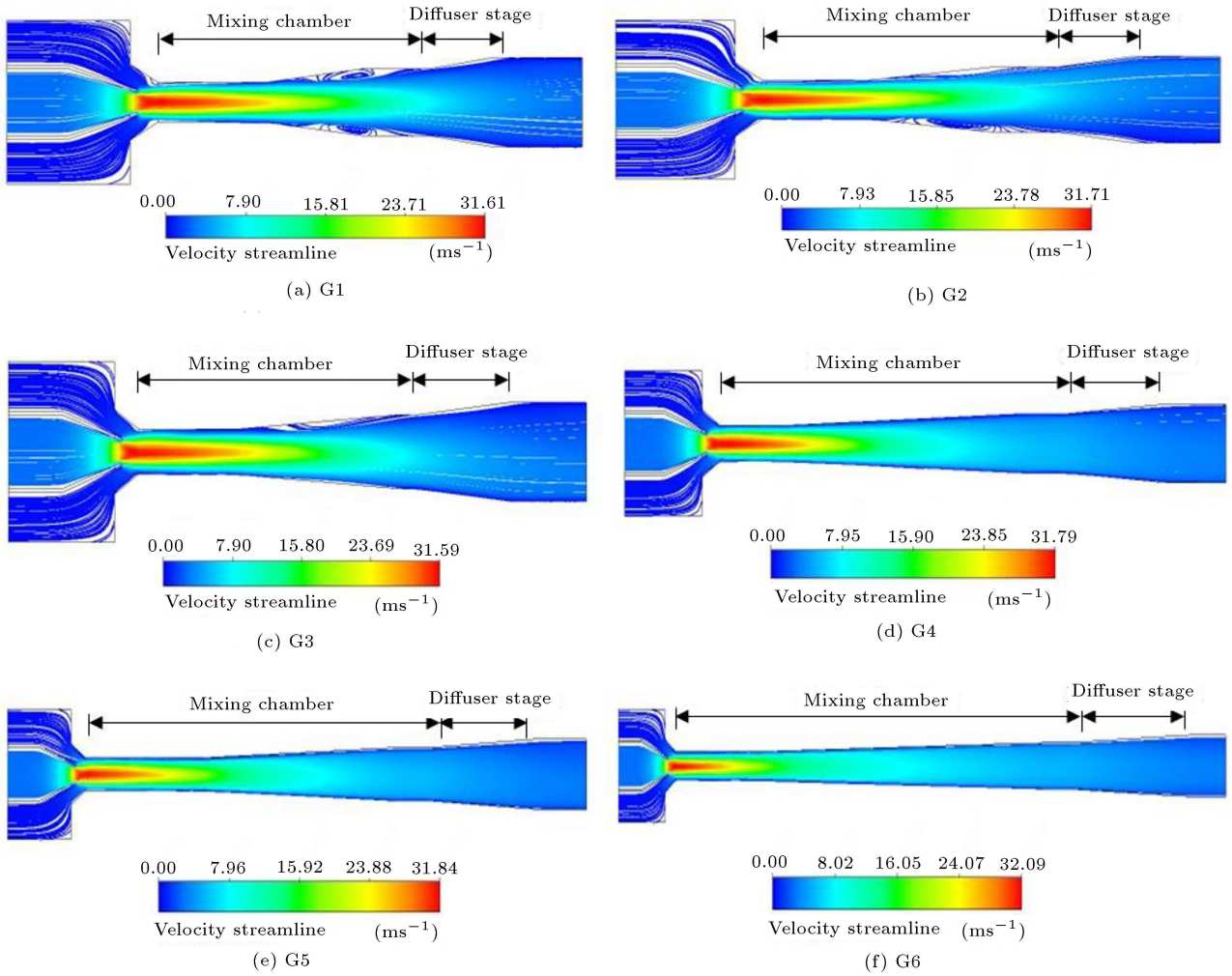

Figure 14. Velocity distribution and streamlines for several configurations of modified mixing chamber system.

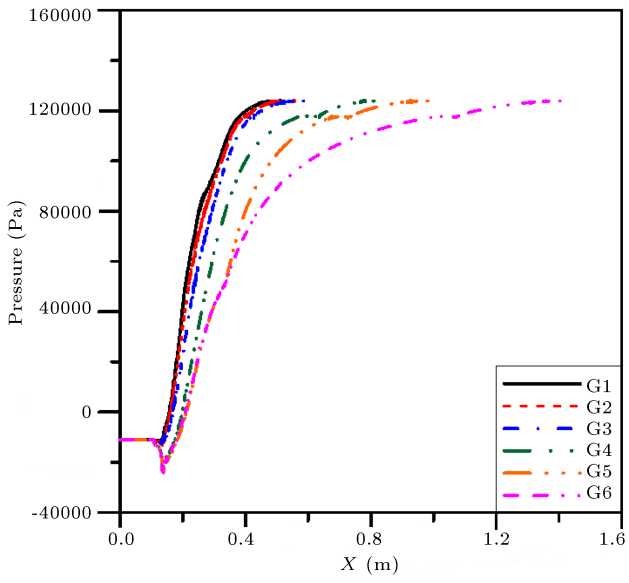

Figure 15. Pressure distribution along the axial-jet-pump outer surface for several configurations of modified mixing chamber system.

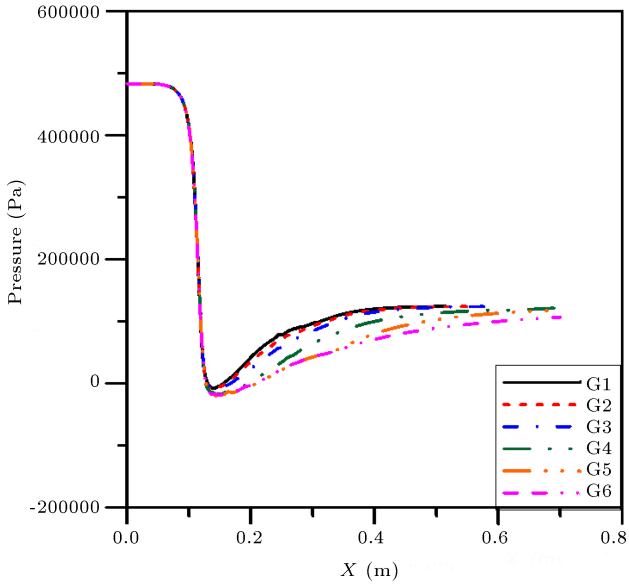

Figure 16. Pressure distribution along the axial-jet-pump center line for several configurations of modified mixing chamber system.

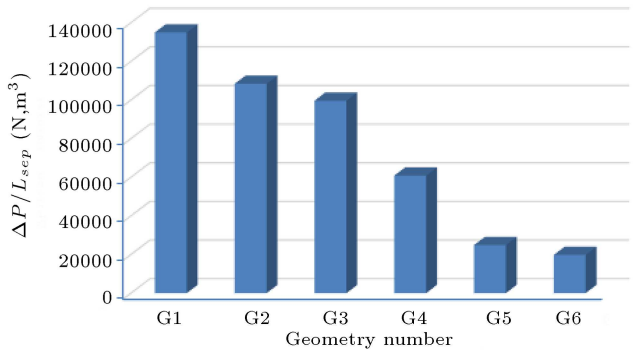

Figure 17. Pressure losses along the separation length for several configurations of modified mixing chamber system.

(G5 and G6) demonstrate the best vacuum pressure in the suction nozzle and the highest entrained fluid when compared to other configurations. Furthermore, (G5) has a better pressure recovery than (G6). As a result, (G5) provides the optimum performance and efficiency.

Figure 17 illustrates the pressure losses along the separation length for several configurations of the modified mixing chamber system. It can be seen that decreasing the angle of the tailpipe diffuser and increasing the pressure recovery length devastate separation that occurs in a diffuser and hence reduces the pressure losses. Even though the pressure losses in configuration (G5) are higher than the losses in configuration (G6), the best performance and highest efficiency are attained in configuration (G5). The reason for the highest efficiency dates back to the better pressure recovery in the tailpipe diffuser corresponding to the optimized diffuser angle. The separation losses in configuration (G6) are the lowest compared with other configurations, but the friction losses increase due to the increasing length of the tailpipe diffuser.

7. Conclusions

In the present study, a numerical investigation is carried out for the axial jet-pump with different mixing chamber configurations. The comparison of experimental data found in the literature with the current numerical outcomes served to validate the current numerical study. One of the study's important achievements is to discover the factors that result in significant losses occurring at the point where motive and entrained fluids collide, as well as the dependency of these losses on mixing chamber shape. One of the strongest attributes of the current work is overcoming the partial mixing before the mixed fluid reaches the tail-diffuser. The newly suggested modification of the mixing chamber geometry can offset this loss at intermediate flowrates (moderate flow rate ratios). In the case of a non-swirling flow, the creation of a recirculation area near the inlet of the mixing chamber is another factor contributing to greater loss. The main conclusions drawn from the present study are:

1. The axial-jet-pump geometry has a frank effect on the flow parameters (i.e., pressure, fluid velocity) and the pump performance;
2. The mixing process for the constant-diffuser-constant mixing chamber is much better than the constant mixing chamber axial-jet-pump configuration;
3. The introduction of a swirl at the inlet to the suction chamber is suitable for controlling the mixing loss in the jet pump;
4. The optimum degree of swirl is found to be 45° which increases the jet pump efficiency by 12.76% compared with the same pump configuration with zero-swirl;
5. Adding a swirl in the motive line degrades the pump performance due to increasing the mixing loss in the jet pump;
6. The maximum efficiency of 38.08% was achieved for the mixing chamber (constant-diffuser-constant) by engendering a swirl in the suction chamber with 45° of swirl;
7. The optimum angle of the tailpipe diffuser is found to be 3°.

Subscripts

d	Discharge/outlet
n	Nozzle
m	Motive/primary fluid
t	Mixing pipe
s	Suction, smooth
dif_1.	1st diffuser stage
dif_2.	2nd diffuser stage
sep	Separation

Nomenclature

x_i	Coordinate (m)
x_n	Driving nozzle position (m)
M_r	Flow rate ratio ($\dot{m}_s/\dot{m}_m$)
P_r	Pressure ratio
Ω	Specific turbulent dissipation rate (s^{-1})
u_i	Time-averaged velocity (m/s)
μ_t	Turbulent viscosity (Pa.s)
$E_{\gamma 1}$	Transition source
$P_{\gamma 1}$	Transition source
$E_{\gamma 2}$	Destruction source

$P_{\gamma 2}$	Relaminarization source
$P_{\theta t}$	Source term
$\tilde{D}_k$	Destruction term for the turbulence model
$\tilde{P}_k$	Production term for the turbulence model
$c_{\theta t}$	Constant
$\sigma_{\theta t}$	Constant
y^+	Non-dimensional parameter
μ	Dynamic viscosity (Pa.s)
D	Diameter (m)
ε	Turbulent kinetic energy dissipation (m^2/s^3)
K_s	Roughness height (mm)
K	Turbulent kinetic energy (m^2/s^2)
l	Length (m)
L	Relative length of mixing chamber
P	Static pressure (kPa)
Re	Reynolds number
X	Distance from the jet pump inlet (m)
y	The normal distance from wall (m)
Z	Relative position of driving nozzle (x_n/d_n)
η	Jet pump efficiency
P	Fluid density (kg/m^3)
$\grave{u}$	Fluctuation velocity component (m/s)
v	Kinematic viscosity (m^2/s)
$\dot{m}$	Mass flow rate (kg/s)

References

1. Schulz, F., *Modellversuchefür Wasserstrahl-Wasserpumpen*, Habil, TU, Wien (1952).
2. Schulz, H., *Die Pumpen*, Springer Verlag (1977).
3. Raabe, J., *Hydraulische Maschinen und Anlagen*, VDI Verlag (1989).
4. Hefny, M.M. "An experimental investigation of jet pumps with swirling components in the driving jet flow", MSc Thesis, High Institute of Energy, Aswan, Egypt (2002).
5. Gelany, A.M. "An experimental investigation of jet pumps with multiple jets in the driving jet flow", MSc Thesis, High Institute of Energy, Aswan, Egypt (2004).
6. Shimizu, Y., Nakamura, S., Kuzuhara, S., et al. "Studies of the configuration and performance of annular type jet pumps", *Trans. Jpn. Soc. Mech. Eng.*, **49**, 2746 (1983).
7. Guillaume, D.W. and Judge, T.A. "Improving the efficiency of a jet pump using a swirling primary jet", *Review of Scientific Instruments*, **75**(2), pp. 553–555 (2004).
8. Zhou, B., Fleck, B., Bouak, F., et al. "Comparison of swirling effects on ejector performance using four turbulence models", *Canadian Aeronautics and Space Journal*, **46**(4), pp. 178–182 (2000).
9. Yamamoto, M., Maeda, T., and Kitamura, O. "Computation of performance of annular jet pump with and without inlet swirl", In *Proceedings of the ASME Fluids Engineering Division Summer Meeting*, ASME paper, S269-4865: pp. 1–9 (1998).
10. Panevnyk, D.O. "The study on the flows kinematics in the jet pump's mixing chamber", Natsional'nyi Hirnychyi Universytet, Naukovyi Visnyk 1, pp. 62–68 (2019).
11. De Jesús Portillo-Vélez, R., Vásquez-Santacruz, J.A., Marín-Urías, L.F., et al. "Efficiency maximization of a jet pump for a hydraulic artificial lift system", *Revista Internacional de Métodos Numéricos Para Cálculo y Diseño en Ingeniería*, **35**(1), pp. 1–13 (2019).
12. Aldas, K. and Yapici, R. "Investigation of effects of scale and surface roughness on efficiency of water jet pumps using CFD", *Engineering Applications of Computational Fluid Mechanics*, **8**(1), pp. 14–25 (2014).
13. Wang, X., Chen, Y., Li, M., et al. "Numerical study on the working performance of a streamlined annular jet pump", *Energies*, **13**(17), p. 4411 (2020).
14. Brijesh, R.N. and Sagar, M.P. "The effect of venturi design on jet pump performance", *Journal for Research*, **2**(4), pp. 23–28 (2016).
15. Xiaogang, D., Jingliang, D., Zhentao, W., et al. "Numerical analysis of an annular water-air jet pump with self-induced oscillation mixing chamber", *The Journal of Computational Multiphase Flows*, **9**(1), pp. 47–53 (2017).
16. Zhu, H.Y. and Liu, Q.Y. "Pressure drawdown mechanism and design principle of jet pump bit", Scientia Iranica, Transactions B: Mechanical Engineering, **22**(3), pp. 792–803 (2015).
17. Wang, X.D., Chen, Y.L., Zhao, Y., et al. "Influence of suction chamber profile on flow field of annular jet pump", *International Conference on Civil and Hydraulic Engineering*, **304**, 032088 (2019).
18. Xu, K., Wang, G., Wang, L., et al. "Parameter analysis and optimization of annular jet pump based on kriging model", *Applied Science*, **10**, 7860 (2020).
19. Helios, M.P. and Asvapoositkul, W. "An experimental study of the effect of the projection ratio and throat-aspect ratio on the efficiency and loss coefficient of a water jet pump", *Journal of Mechanical Engineering and Sciences*, **15**(3), pp. 8277–8288 (2021).
20. Murillo, W.O., Arcila, I.D.P., and Palacio-Fernández, J.A. "Geometric optimization of jet pump used in vacuum distillation applications under different operating conditions using genetic-algorithm methods", *Journal of Applied and Computational Mechanics*, **8**(1), pp. 340–358 (2022).

21. Wang, X., Chen, Y., Li, M., et al. "Numerical investigation of the cavitation performance of annular jet pumps with different profiles of suction chamber and throat inlet", *Engineering Applications of Computational Fluid Mechanics*, **14**(1), pp. 1416–1428 (2020).

22. Gao, G., Xing, Y., and Wang, Y. "Effect of nozzle throat geometry on flow field in liquid gas jet pump: A simulation study", *Chin. J. Vac. Sci. Technol.*, **40**, pp. 174–179 (2020).

23. Xu, K., Wang, G., Zhang, L., et al. "Multi-objective optimization of jet pump based on RBF neural network model", *Journal of Marine Science and Engineering*, **9**(2), 236 (2021).

24. Toteff, J., Asuaje, M., and Noguera, R. "New design and optimization of a jet pump to boost heavy oil production", *Computation Journal*, **10**(1), p. 11 (2022).

25. ANSYS® FLUENT, Release 17.0, User's Guide Contents, Fluent, Theory Guide, Turbulence and Single-phase Models, Inc. documentation help.

26. Sheha, A.A.A. "Study of jet pump performance", MSc Thesis, Faculty of Engineering, Menoufia University, Egypt (2017).

27. Sheha, A.A.A., Nasr, M., Hosien, M.A., et al. "Computational and experimental study on the water-jet pump performance", *Journal of Applied Fluid Mechanics*, **11**(4), pp. 1013–1020 (2018).

28. Langtry, R.B., Menter, F.R., Likki, S.R., et al. "A correlation-based transition model using local variables, part-2-test cases and industrial applications", In *Proceedings of the ASME Turbo Expo.*, Vienna, Austria, GT2004-53454: pp. 14–17 (2004).

29. Menter, F.R., Langtry, R.B., Likki, S.R., et al. "A correlation based transition model using local variables, Part-1- model formulation", In *Proceedings of the ASME Turbo Expo.*, Vienna, Austria, GT2004-53452: pp. 14–17 (2004).

30. Menter, F.R., Langtry, R.B., and Völker, S. "Transition modeling for general purpose CFD codes", *Flow Turbul. Combust.*, **77**(1–4), pp. 277–303 (2006).

31. Xie, Z., Wang, X., and Zhu, W. "Theoretical and experimental exploration into the fluid structure coupling dynamic behaviors towards water-lubricated bearing with axial asymmetric grooves", *Mechanical Systems and Signal Processing*, **168**, 108624 (2022).

32. Xie, Z. and Zhu, W. "Theoretical and experimental exploration on the micro asperity contact load ratios and lubrication regimes transition for water-lubricated stern tube bearing", *Tribology International*, **164**, 107105 (2021).

33. Lin, Q., Wei, Z., Wang, N., et al. "Analysis on the lubrication performances of journal bearing system using computational fluid dynamics and fluid-structure interaction considering thermal influence and cavitation", *Tribology International*, **64**, pp. 8–15 (2013).

34. Rocklage-Marliani, G., Schmidts, M., and Vasanta-Ram, V.I. "Three-dimensional laser-doppler velocimeter measurements in swirling turbulent pipe flow", *Flow Turbulence and Combustion*, **70**, pp. 43–67 (2003).

Biographies

Ahmed Abdelaziz Ahmed Sheha is a PhD student in the faculty of engineering at Menoufia University, Egypt. He works as a Mechanical Section Head and Rotating Equipment Engineer at PetroGulf Misr Petroleum Company. He has worked as a consultant in many petroleum projects, following up on the implementation and delivery of the project. His research interests are in the fields of fluid mechanics, jet pumps, CFD, and off-shore petroleum engineering applications. He published research in the field of axial-jet-pump.

Kamal Abdelaziz Ibrahim is a Professor of mechanical power engineering at the faculty of engineering, Menoufia University, Egypt. His research interests are in the fields of Fluid Mechanics, Turbo-Machinery, Wind Energy, Two-Phase-Flow, and CFD. He published several researches in different international journals.

Hassan Awad Abdalla is a Professor of mechanical power engineering at the faculty of engineering at Menoufia University, Egypt. His research interests are in the fields of Fluid Mechanics, Two-Phase-Flow, Turbo-Machinery, Wind energy, Gas turbines, and CFD. He published several researches in different international journals.

Samy Mohammed El-Behery is an Associate Professor of mechanical power engineering at the faculty of engineering at Menoufia University, Egypt. His research interests are in the fields of Fluid Mechanics, Two-Phase-Flow, Combustion engines, Turbo-Machinery, and CFD. He published several researches in different international journals.

Ismail Mohamed Sakr is an Associate Professor of mechanical power engineering at the faculty of engineering at Menoufia University, Egypt. His research interests are in the fields of Fluid Mechanics, Two-Phase-Flow, Wind Energy, Hydrogen Energy, and CFD. He published several researches in different international journals.